

Modified scaling angular spectrum method for numerical simulation in long-distance propagation

Xiao-Yi Chen(陈晓义), Ya-Xuan Duan(段亚轩), Bin-Bin Xiang(项斌斌), Ming Li(李铭), and Zheng-Shang Da(达争尚)

Citation: Chin. Phys. B, 2021, 30 (**3**): 034203. DOI: 10.1088/1674-1056/abd38d
Journal homepage: http://cpb.iphy.ac.cn; http://iopscience.iop.org/cpb

What follows is a list of articles you may be interested in

Generation of Mathieu beams using angular pupil modulation

Zhijun Ren(任志君), Jinping He(何晋平), Yile Shi(施逸乐)
Chin. Phys. B, 2018, 27 (**12**): 124201. DOI: 10.1088/1674-1056/27/12/124201

Nonuniform sampled angular spectrum method by using trigonometric interpolation

Qiu-Hu Cheng(程秋虎), Shi-Yu Wang(王石语), Meng-Yao Wu(吴梦瑶), Zhen Guo(过振), De-Fang Cai(蔡德芳), Bing-Bin Li(李兵斌)
Chin. Phys. B, 2018, 27 (**9**): 094203. DOI: 10.1088/1674-1056/27/9/094203

Near-field characteristics of highly non-paraxial subwavelength optical fields with hybrid states of polarization

Rui-Pin Chen(陈瑞品), Teng-Yue Gao(高腾跃), Khian-Hooi Chew(周健辉), Chao-Qing Dai(戴朝卿), Guo-Quan Zhou(周国泉), Sai-Ling He(何赛灵)
Chin. Phys. B, 2017, 26 (**10**): 104202. DOI: 10.1088/1674-1056/26/10/104202

Reflection and transmission of Laguerre Gaussian beam from uniaxial anisotropic multilayered media

Hai-Ying Li(李海英), Zhen-Sen Wu(吴振森), Qing-Chao Shang(尚庆超), Lu Bai(白璐), Zheng-Jun Li(李正军)
Chin. Phys. B, 2017, 26 (**3**): 034204. DOI: 10.1088/1674-1056/26/3/034204

Analysis of the spatial filter of a dielectric multilayer film reflective cutoff filter-combination device

Zhang Ying, Qi Hong-Ji, Yi Kui, Wang Yan-Zhi, Sui Zhan, Shao Jian-Da
Chin. Phys. B, 2015, 24 (**10**): 104216. DOI: 10.1088/1674-1056/24/10/104216

Modified scaling angular spectrum method for numerical simulation in long-distance propagation*

Xiao-Yi Chen(陈晓义)[1,2], Ya-Xuan Duan(段亚轩)[1,†], Bin-Bin Xiang(项斌斌)[3], Ming Li(李铭)[1], and Zheng-Shang Da(达争尚)[1]

[1] *The Advanced Optical Instrument Research Department, Xi'an Institute of Optics and Precision Mechanics, Chinese Academy of Sciences, Xi'an* 710119, *China*

[2] *University of Chinese Academy of Sciences, Beijing* 100049, *China*

[3] *Xinjiang Astronomical Observatory, Chinese Academy of Sciences, Urumqi* 830011, *China*

(Received 18 September 2020; revised manuscript received 28 October 2020; accepted manuscript online 15 December 2020)

The angular method (AS) cannot be used in long-distance propagation because it produces severe numerical errors due to the sampling problem in the transfer function. Two ways can solve this problem in AS for long-distance propagation. One is zero-padding to make sure that the calculation window is wide enough, but it leads to a huge calculation burden. The other is a method called band-limited angular spectrum (BLAS), in which the transfer function is truncated and results in that the calculation accuracy decreases as the propagation distance increases. In this paper, a new method called modified scaling angular spectrum (MSAS) to solve the problem for long-distance propagation is proposed. A scaling factor is introduced in MSAS so that the sampling interval of the input plane can be adjusted arbitrarily unlike AS whose sampling interval is restricted by the detector's pixel size. The sampling interval of the input plane is larger than the detector's pixel size so the size of calculation window suitable for long-distance field propagation in the input plane is smaller than the size of the calculation window required by the zero-padding. Therefore, the method reduces the calculation redundancy and improves the calculation speed. The results from simulations and experiments show that MSAS has a good signal-to-noise ratio (SNR), and the calculation accuracy of MSAS is better than BLAS.

Keywords: angular spectrum, diffraction, Fourier optics and signal process

PACS: 42.30.Kq, 42.30.Rx, 42.30.–d **DOI:** 10.1088/1674-1056/abd38d

1. Introduction

Digital simulation of scalar diffraction is widely used for studies like phase retrieval,[1–6] digital holography,[7,8] optical information security,[9] and computational imaging.[10,11] These simulations of diffraction are usually based on the well-known scalar diffraction theories. For parallel planes,[12] there are mainly three methods of field propagation called the single Fourier-transform-based Fresnel method (SFT-FR), the convolution-based Fresnel method (CV-FR), and the AS method respectively. The SFT-FR has the fastest speed, but the sampling interval is proportional to the propagation distance. To control the sampling interval, the multi-step Fresnel method[13–15] and shifted Fresnel method (shift-FR)[16] have been proposed. The CV-FR and AS are all convolution-based methods, so the sampling window and the sampling interval in the input plane are the same as those in the output plane. Compared with CV-FR, AS is more accurate as it is directly derived from Rayleigh–Sommerfeld diffraction theory without approximation.[17,18] But the sampling problem in the transfer function makes that AS only accurate for quite near field. However, the long-distance propagation often occurs in some applications such as wavefront detection, computational holography, and antenna detection.

There are two effective methods to achieve long-distance propagation based on AS. One is adding a wide calculation window (zero-padding) in the input plane, which will lead to large amount of calculation. The other is BLAS[19] method, in which the transfer function is truncated to a proper bandwidth. The aliasing transfer function components are forced to be zeros and only the non-aliasing transfer function components are used. It has been shown that the effective non-aliasing bandwidth of the transfer function would decrease rapidly when the propagation distance increases. So, the accuracy of BLAS in inverse calculation from the output plane to the input plane decreases as the propagation distance increases.[19,20] Therefore, the application of BLAS in iterative phase retrieval technology is limited.

In this paper, a modified scaling angular spectrum (MSAS) method for long-distance propagation is proposed. It consists of two parts, the scaling calculation and the choice of calculation window. Firstly, a scaling factor is introduced so that the sampling interval of input plane can be defined independently. And by applying the Bluestein substitution, the discrete Fourier transform can be used even if the sampling intervals of input plane are different from that of output

*Project supported by the National Natural Science Foundation of China (Grant No. 61705254) and the Key Research and Development Program of Shaanxi Province of China (Grant No. 2020GY-114).

†Corresponding author. E-mail: duanyaxuan@opt.ac.cn

© 2021 Chinese Physical Society and IOP Publishing Ltd

plane.[21–24] The calculation speed of MSAS is fast because it is based on a linear convolution which can be evaluated by fast Fourier transform (FFT) effectively. Then the most suitable size of the calculation window is selected so that the numerical calculation in long-distance propagation runs efficiently. Unlike the truncation of the transfer function in BLAS method, the proposed method can also be accurately calculated in the inverse calculation.

The rest of this paper is arranged as follows: In Section 2, the principle of traditional long-distance propagation is introduced in details. Section 3 discusses the MSAS proposed in this paper and explains it from three parts: the scaling calculation of MSAS, the calculation window of MSAS, and computational complexity. In Section 4, MSAS is compared with other methods when used for numerical calculation in long-distance propagation. In Section 5, the simulations are verified through experiments. Finally, in Section 6, conclusions are drawn.

2. The principle of the traditional long-distance propagation

In the scalar diffraction theory, the accurate diffraction formula is the Rayleigh–Sommerfeld diffraction integral. It is always converted into a convolution form which is also called the AS formula

$$U(x,y,z) = F^{-1}\{F[U_0(x_0,y_0,0)]H(u,v,z)\}, \tag{1}$$

where z is the propagation distance, (x_0,y_0) and $U_0(x_0,y_0,0)$ are the coordinates and the light field of input plane, (x,y) and $U(x,y,z)$ are the coordinates and the light field of output plane, F and F^{-1} represent the Fourier transform and inverse Fourier transform, respectively. $H(u,v,z)$ is the transfer function,

$$H(u,v,z) = \exp\left[\mathrm{i}2\pi z\left(\lambda^{-2}-u^2-v^2\right)^{1/2}\right], \tag{2}$$

where λ is the wavelength, u and v are the Fourier frequencies in x and y directions, respectively.

The calculation of AS is based on the discrete Fourier transform (DFT) which only describes the discrete periodic function. As shown in Fig. 1, the sampling of the input field would result in the generation of modulated and translated replicas in periodic locations of the input plane. To avoid the aliasing error, the discrete calculation of Eq. (1) need to meet Nyquist sampling theorem. So the discrete transfer function's sampling rate of change is less than or equal to π when $m = M/2$, $n = N/2$, we obtain[25]

$$\left|\frac{\partial}{\partial m}2\pi z\sqrt{\lambda^{-2}-\left(\frac{m}{M\Delta x_0}\right)^2-\left(\frac{n}{N\Delta y_0}\right)^2}\right|_{m=M/2,n=N/2} \le \pi, \tag{3}$$

where $m = -M/2,-M/2+1,\ldots,M/2-1$ and $n = -N/2,-N/2+1,\ldots,N/2-1$, M and N are the sampling numbers in the x_0 and y_0 directions, Δx_0 and Δy_0 are the sampling intervals in the x_0 and y_0 directions, respectively. Therefore, the propagation distance z need to satisfy

$$z \le \min\left[M(\Delta x_0)^2/\lambda, N(\Delta y_0)^2/\lambda\right]. \tag{4}$$

In AS, the sampling intervals of the input plane are equal to the sampling intervals of the output plane. Meanwhile, the sampling intervals of the output plane are determined by the pixel sizes of detector. Once the pixel sizes of the detector $(\Delta x, \Delta y)$ are determined, the sampling intervals of input plane $(\Delta x_0 = \Delta x,\ \Delta y_0 = \Delta y)$ are also determined accordingly. According to Eq. (4), the propagation distance is restricted to a limited value.

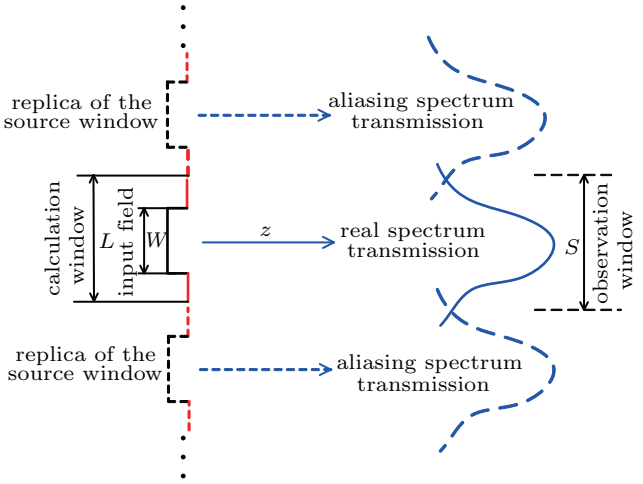


Fig. 1. Replicas of the physical window in the input plane.

Obviously, the most direct way to achieve long-distance propagation is increasing the sampling numbers with zero-padding, which is called PAS method in this paper. When the propagation distance z is determined, the sampling numbers required for PAS meet the following condition. The increase in sampling numbers brings a huge computational burden.

$$M_{\mathrm{PAS}} \ge \lambda z/(\Delta x_0)^2, \quad N_{\mathrm{PAS}} \ge \lambda z/(\Delta y_0)^2. \tag{5}$$

Another way is to truncate the transfer function to a limited bandwidth, which is called BLAS. The expression of its transfer function is[19]

$$H'(u,v,z) = H(u,v,z)\,\mathrm{rect}\left(\frac{u}{2u_{\mathrm{lim}}}\right)\mathrm{rect}\left(\frac{v}{2v_{\mathrm{lim}}}\right), \tag{6}$$

where u_{lim} and v_{lim} are

$$u_{\mathrm{lim}} = \frac{1}{\left[(2\Delta u z)^2+1\right]^{1/2}\lambda}, \quad v_{\mathrm{lim}} = \frac{1}{\left[(2\Delta v z)^2+1\right]^{1/2}\lambda}, \tag{7}$$

where $\Delta u = 1/[2(M\Delta y_0)]$, $\Delta v = 1/[2(N\Delta y_0)]$. Although BLAS increases the propagation distance, high-frequency information is lost due to the limited bandwidth in the frequency domain and the accuracy in inverse calculation is also limited.

3. Modified scaling angular spectrum propagation

3.1. Scaling calculation of MSAS

From Eq. (4), the propagation distance is also related to the sampling intervals in the input plane. As the sampling intervals increase, the propagation distance increases. However, the sampling intervals between the input plane and the output plane are equal in traditional long-distance propagation. Therefore, MSAS consists of two parts: the scaling calculation and the selection of calculation window. One is to freely define the sampling interval of the input plane, and the other is to select the most suitable size of calculation window for long-distance propagation.

MSAS is derived from AS, and the coordinate system used in formulas is shown in Fig. 2. P and Q are the sampling numbers of calculation window in the x_0 and y_0 directions, respectively. R and T are the sampling points of the input field in the x_0 and y_0 directions, respectively. The discrete Fourier transform of the input plane $A(u_p, v_q, 0)$ can be expressed as

$$A(u_p,v_q,0) = \sum_{p=-P/2}^{p=P/2}\sum_{q=-Q/2}^{q=-Q/2} U_0(x_{0p},y_{0q},0) \times \exp\left[-\mathrm{i}2\pi\left(u_p x_{0q}+v_q y_{0q}\right)\right]\Delta x_0\Delta y_0, \quad (8)$$

where $x_{0p} = p\Delta x_0$, $y_{0q} = q\Delta y_0$, $u_p = p\Delta u$, and $v_p = q\Delta v$. So, the diffraction field of output plane is

$$U(x_r,y_t,z) = \sum_{r=-R/2}^{r=R/2}\sum_{t=-T/2}^{t=T/2} A(u_p,v_q,z) \times \exp\left[\mathrm{i}2\pi\left(u_p x_r+v_q y_t\right)\right]\Delta u\Delta v, \quad (9)$$

where

$$A(u_p,v_q,z) = A(u_p,v_q,0)\,H(u_p,v_q,z)$$

is discrete Fourier transform of the output plane, $x_r = r\Delta x$, $y_t = t\Delta y$. Δx and Δy are the sampling intervals of output plane in x and y directions, respectively. We cannot directly use the inverse discrete Fourier transform to calculate the summation of Eq. (9) because of the differences of the sample intervals and sampling numbers in the input and output planes ($P \neq R$, $Q \neq T$, $\Delta x \neq \Delta x_0$, $\Delta y \neq \Delta y_0$). To solve this problem, a scaling factor h is firstly introduced into Eq. (9) as

$$U(x_r,y_t,z) = \sum_{r=-R/2}^{r=R/2}\sum_{t=-T/2}^{t=T/2} A(u_p,v_q,z) \times \exp\left[\frac{\mathrm{i}\pi}{h}\left(2hu_p x_r+2hv_q y_t\right)\right]\Delta u\Delta v. \quad (10)$$

Additionally, the term $(2hu_p x_r + 2hv_q y_t)$ can be converted to the following expression:

$$-[(hu_p-x_r)^2+(hv_q-y_t)^2-\left(x_r^2+y_t^2\right)-(hu_r)^2-(hv_t)^2],$$

which is known as Bluestein substitution.[22] Then the summation process in Eq. (10) is converted into a discrete convolution

$$\begin{aligned} &U(x_r,y_t,z)\\ &= \sum_{r=-R/2}^{r=R/2}\sum_{t=-T/2}^{t=T/2} A(u_p,v_q,z)\Delta u\Delta v\\ &\quad\times\exp\left\{-\frac{\mathrm{i}\pi}{h}\left[(hu_p-x_r)^2+(hv_q-y_t)^2\right.\right.\\ &\quad\left.\left.-\left(x_r^2+y_t^2\right)-(hu_p)^2-(hv_q)^2\right]\right\}\\ &= \sum_{r=-R/2}^{r=R/2}\sum_{t=-T/2}^{t=T/2}\frac{1}{h^2}A(u_p,v_q,z)\exp\left[\frac{\mathrm{i}\pi}{h}\left(x_r^2+y_t^2\right)\right]\\ &\quad\times\exp\left\{\frac{\mathrm{i}\pi}{h}\left[(hu_p)^2+(hv_q)^2\right]\right\}\\ &\quad\times\exp\left\{-\frac{\mathrm{i}\pi}{h}\left[(hu_p-x_r)^2+(hv_q-y_t)^2\right]\right\}h^2\Delta u\Delta v\\ &= \exp\left[\frac{\mathrm{i}\pi}{h}\left(x_r^2+y_t^2\right)\right]\Delta x\Delta y\left[f_1(u',v')*f_2(u',v')\right], \end{aligned} \quad (11)$$

where

$$u' = hu_p, \quad v' = hv_q,$$
$$f_1(u',v') = \left(1/h^2\right)A(u_p,v_q,z)\exp\left\{\mathrm{i}\pi[(hu_p)^2+(hv_q)^2]/h\right\},$$
$$f_2(u',v') = \exp\{-\mathrm{i}\pi[(hu_p)^2+(hv_q)^2/h\},$$

the star operator "$*$" denotes the discrete convolution operation.

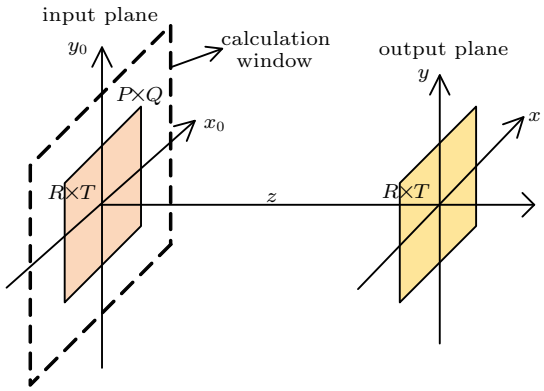


Fig. 2. Geometry of the propagation model between input plane and output plane.

Due to $\Delta u' = \Delta x$, $\Delta v' = \Delta y$, the discrete convolution can also be effectively evaluated by FFT. By Eq. (11), we can choose the independent sampling intervals in the input plane. Meanwhile, the sampling numbers between the input plane and the output plane need not be the same because of the linear convolution. As for the inverse propagation, just let z equal $-z$ and exchange the position of Δx_0 and Δx, Δy_0 and Δy, the calculation formula is still the same as Eq. (11).

The sampling intervals of input plane can be smaller than, equal to, or larger than the sampling intervals of output plane. However, $\Delta x_0 > \Delta x$ and $\Delta y_0 > \Delta y$ are required for long-distance propagation in MSAS to reduce the sampling numbers of calculation window. According to Eq. (4), when the distance is constant, the sampling intervals of the input plane must meet the following condition:

$$\Delta x_0 \geq \sqrt{\lambda z/R}, \quad \Delta y_0 \geq \sqrt{\lambda z/T}. \quad (12)$$

3.2. Calculation window of MSAS

Similarly, a suitable calculation window should be selected in MSAS to make sure that the sampling in the frequency domain is effective for long-distance propagation. In MSAS, increasing the sampling interval in the input plane will reduce the sampling number of the calculation window, so the amount of calculation will be greatly reduced. Taking x_0 and x axes as examples, y_0 and y axes can be analogical.

Firstly, the range of sampling frequency in the transfer function within which no aliasing error occurs must be determined by Eq. (7).[19] The required sampling interval Δu of frequency domain is

$$\Delta u = 1/L_{1x} = 2u_{\text{lim}}/R. \tag{13}$$

Therefore, according to Eqs. (7) and (13), the size of the calculation window is

$$L_{1x} = \frac{2\sqrt{2}zR\lambda}{\sqrt{-R^2\lambda^2 + \sqrt{R^4\lambda^4 + 64z^2R^2\lambda^2}}}. \tag{14}$$

Secondly, to convert a circular convolution to a linear convolution, the input field needs to be doubled both in x and y axes.[21,22]

$$L_{2x} = 2W_x. \tag{15}$$

In addition, FFT will broaden the spectrum of input field. In order to ensure that the aliasing spectrum will not overflow into the output plane, the size of calculation window needs to satisfy[26]

$$L_{3x} = W_x + S_x, \tag{16}$$

where $W_x = R\Delta x_0$ and $S_x = R\Delta x$ are the size of input field and observation window in x_0 and x directions, respectively.

In summary, the calculation window L_x will be the maximum of L_{1x}, L_{2x} and L_{3x} for meeting all these requirements from Eqs. (14)–(16). P can be obtained by L_x, Δx_0, and Q is analogical.

$$L_x = \max\left(L_{1x}, L_{2x}, L_{3x}\right). \tag{17}$$

As shown in Fig. 3, the highest spatial frequency observed at the upper end of observation window may be given by the field coming from the lower end of the input field. Therefore, the minimum bandwidth of the spectrum which is needed for exact numerical propagation is

$$u_{\text{need}} = \frac{\sin\theta_x}{\lambda} = \frac{1}{\lambda\left[\left(2z/(W_x+S_x)\right)^2+1\right]^{1/2}}. \tag{18}$$

After adding the calculation window by Eq. (17), the maximum bandwidth which MSAS can be correctly sampled is[19,27]

$$u_{\max} = \frac{1}{\lambda\left[\left(2z/L_x\right)^2+1\right]^{1/2}}. \tag{19}$$

If $u_{\max} < u_{\text{need}}$, the input field loses a part of the frequency band necessary for exact diffraction. Therefore, for an accurate sample, the relation between $u_{\max}$ and u_{need} is

$$u_{\max} \geq u_{\text{need}}. \tag{20}$$

From Eqs. (18) and (19), we know the following two points.

(i) if $L = \max\left(L_1, L_2, L_3\right) = L_3$, $u_{\max} = u_{\text{need}}$;

(ii) if $L = \max\left(L_1, L_2, L_3\right) = L_1$ or L_2, $u_{\max} > u_{\text{need}}$.

So equation (20) is always satisfied.

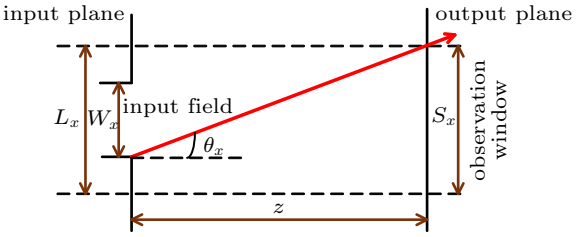


Fig. 3. A model for minimum bandwidth required for exact numerical propagation.

Figure 4 shows a sampled transfer function of AS, where the parameters are $M = 1024$, $z = 50M\Delta x$, $\lambda = 635$ nm, $\Delta x = 2\lambda$, and $\Delta x_0 = 2\lambda$. Only the real part of transfer function is depicted in the sampling interval $\Delta u = 1/M\Delta x_0$ of AS. Because the transfer function is a kind of chirp function, an aliasing error is introduced in the sampled transfer function as shown in Fig. 4. With MSAS method, Δx_0 increases to 10λ and the calculation window is determined by Eq. (17). Then the maximum bandwidth $u_{\max}$ can be calculated by Eq. (19). As a result, the aliasing error is removed.

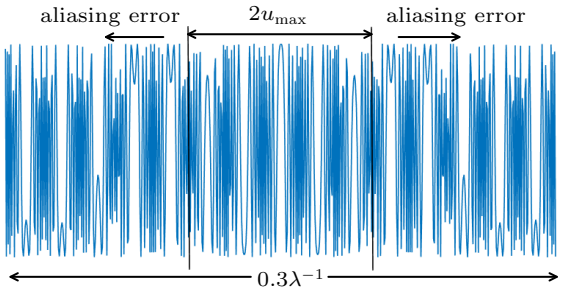


Fig. 4. Example of a sampled transfer function of AS and MSAS.

3.3. Computational complexity

Both the AS and PAS use two Fourier transforms. The computational complexity can be calculated by the following formulas:

$$\begin{aligned} C_{\text{AS}} &= O\left[M\times N\log_2\left(M\times N\right)\right] \\ &\quad + O\left[M\times N\log_2\left(M\times N\right)\right], \end{aligned} \tag{21}$$

$$\begin{aligned} C_{\text{PAS}} &= O\left[M_{\text{PAS}}\times N_{\text{PAS}}\log_2\left(M_{\text{PAS}}\times N_{\text{PAS}}\right)\right] \\ &\quad + O\left[M_{\text{PAS}}\times N_{\text{PAS}}\log_2\left(M_{\text{PAS}}\times N_{\text{PAS}}\right)\right]. \end{aligned} \tag{22}$$

In MSAS, one FFT calculations and one FFT-based linear convolution are used, so the computational complexity is

$$C_{\mathrm{MSAS}} = O\left[P\times Q\log_2\left(P\times Q\right)\right]+O\big\{\left(P+R\right)\times\left(Q+T\right)\log_2\left[\left(P+R\right)\times\left(Q+T\right)\right]\big\}. \quad (23)$$

Under long-distance propagation, the sampling number required by MSAS is less than that required by PAS ($M \le R < P < M_{\mathrm{PAS}}$, $N \le T < Q < N_{\mathrm{PAS}}$), so the computational complexity is low ($C_{\mathrm{AS}} < C_{\mathrm{MSAS}} < C_{\mathrm{PAS}}$) and the calculation speed is faster than PAS. Moreover, as the propagation distance increases, more sampling number is required for PAS and the advantage of MSAS is more significant.

4. Simulation

In order to prove the effectiveness of MSAS, we performed the following simulation and compared it with AS, PAS, and BLAS. The parameters of simulation are as follows: the detector pixel size is $\Delta x = \Delta y = 7.4$ μm, the wavelength is $\lambda = 635$ nm, the width of the square aperture is 0.5 mm, the sampling number of the object plane is chosen to be $M \times N = 200 \times 200$ to convert a circular convolution to a linear convolution.[21,22]

In AS, BLAS, and PAS, the sampling interval of input plane is the same as that of output plane. The sampling number in AS does not change with the propagation distance, which is always $M_{\mathrm{AS}} \times N_{\mathrm{AS}} = 200 \times 200$. However, the sampling number of BLAS is $M_{\mathrm{BLAS}} \times N_{\mathrm{BLAS}} = 400 \times 400$ and the sampling number of PAS (M_{PAS} and N_{PAS}) increases according to Eq. (5).

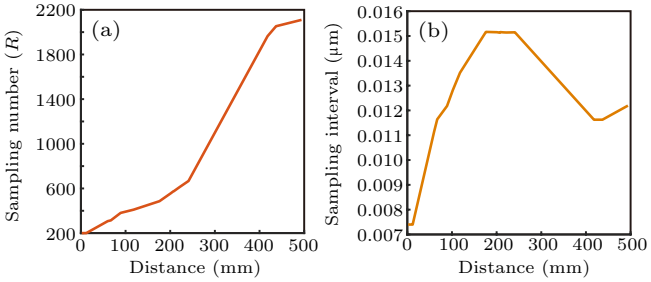


Fig. 5. The minimum sampling number in the diffraction area and the sampling interval of MSAS changes with propagation distance. (a) The minimum sampling number in the diffraction area changes with propagation distance; (b) the sampling interval of MSAS changes with propagation distance.

As the distance increases, the diffractive propagation is divergent. In MSAS, the minimum sampling numbers (R, $T = R$) of diffractive area required for diffraction propagation are determined as shown in Fig. 5(a) according to different diffraction distances. The sampling intervals under different propagation distances in the input plane are determined by the minimum sampling numbers and Eq. (12) as shown in Fig. 5(b). Then the minimum sampling numbers and sampling intervals determine the sampling number (P, $P = Q$) of calculation window.

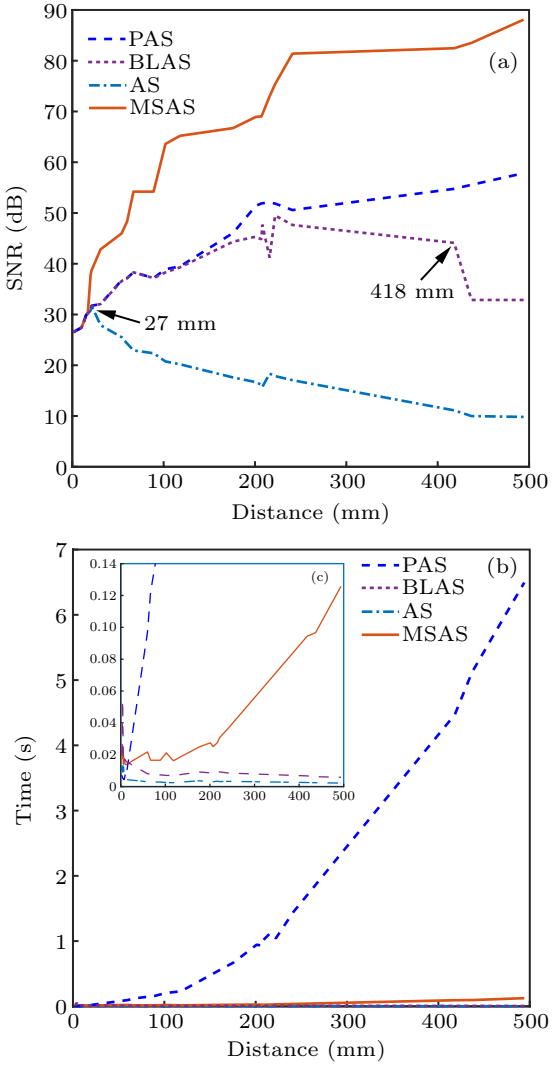


Fig. 6. Comparison of AS, BLAS, PAS, and MSAS. (a) The SNR of AS, BLAS, PAS, and MSAS changes with propagation distance; (b) the calculation time of AS, BLAS, PAS, and MSAS changes with propagation distance; (c) the inset clearly shows calculation time of AS, BLAS, and MSAS when the distance from 0 mm to 500 mm.

Accuracy is evaluated by SNR of the diffraction intensity:[28]

$$\mathrm{SNR} = \frac{\iint_{\infty} I\left(x,y\right)\mathrm{d}x\mathrm{d}y}{\iint_{\infty}\left|I\left(x,y\right)-\alpha I_{\mathrm{rig}}\left(x,y\right)\right|\mathrm{d}x\mathrm{d}y}, \quad (24)$$

where $I\left(x,y\right)$ is the calculated diffraction intensity of output plane obtained by AS, BLAS, PAS or MSAS. $I_{\mathrm{rig}}\left(x,y\right)$ stands for the diffraction intensity on the output plane obtained by the accurate Gauss-quadrature numerical integral (NI) method,[29,30] where α is introduced as follows:

$$\alpha = \frac{\iint_{\infty} I\left(x,y\right)\mathrm{d}x\mathrm{d}y}{\iint_{\infty} I_{\mathrm{rig}}\left(x,y\right)\mathrm{d}x\mathrm{d}y}. \quad (25)$$

As shown in Fig. 6(a), the SNR calculated by BLAS and AS gradually decreases when the distance is larger than 27 mm

and 418 mm respectively. BLAS and AS no longer have an advantage in the long-distance propagation. However, the SNRs of PAS and MSAS tend to increase as the distance increases. PAS and MSAS have very good SNR, but the running speed of MSAS is faster than PAS as the propagation distance increases which is shown in Fig. 6(b). The running speed is consistent with the computational complexity described in Subsection 3.3. In the simulation, MATLAB (Version R2016b, Math Works, Natick, Massachusetts) installed in a 3.40-GHz central processing unit (Intel core i7-6700) and 8 GB of random-access memory desktop computer was used for calculation.

Taking $z_1 = 100$ mm and $z_2 = 500$ mm as examples, the two-dimensional (2D) diffraction intensity, one-dimensional (1D) amplitude, and phase of AS, BLAS, MSAS, PAS, and NI are shown in Fig. 7. When the distance is $z_1 = 100$ mm, the amplitude and phase calculated by AS are already incorrect as shown in Fig. 7(a). However, the amplitude and phase of BLAS, PAS, and MSAS are all consistent with that of NI. When the distance is $z_2 = 500$ mm, BLAS and AS cannot be calculated accurately as shown in Fig. 7(b). But both MSAS and PAS can be calculated accurately like NI, and MSAS runs faster than PAS.

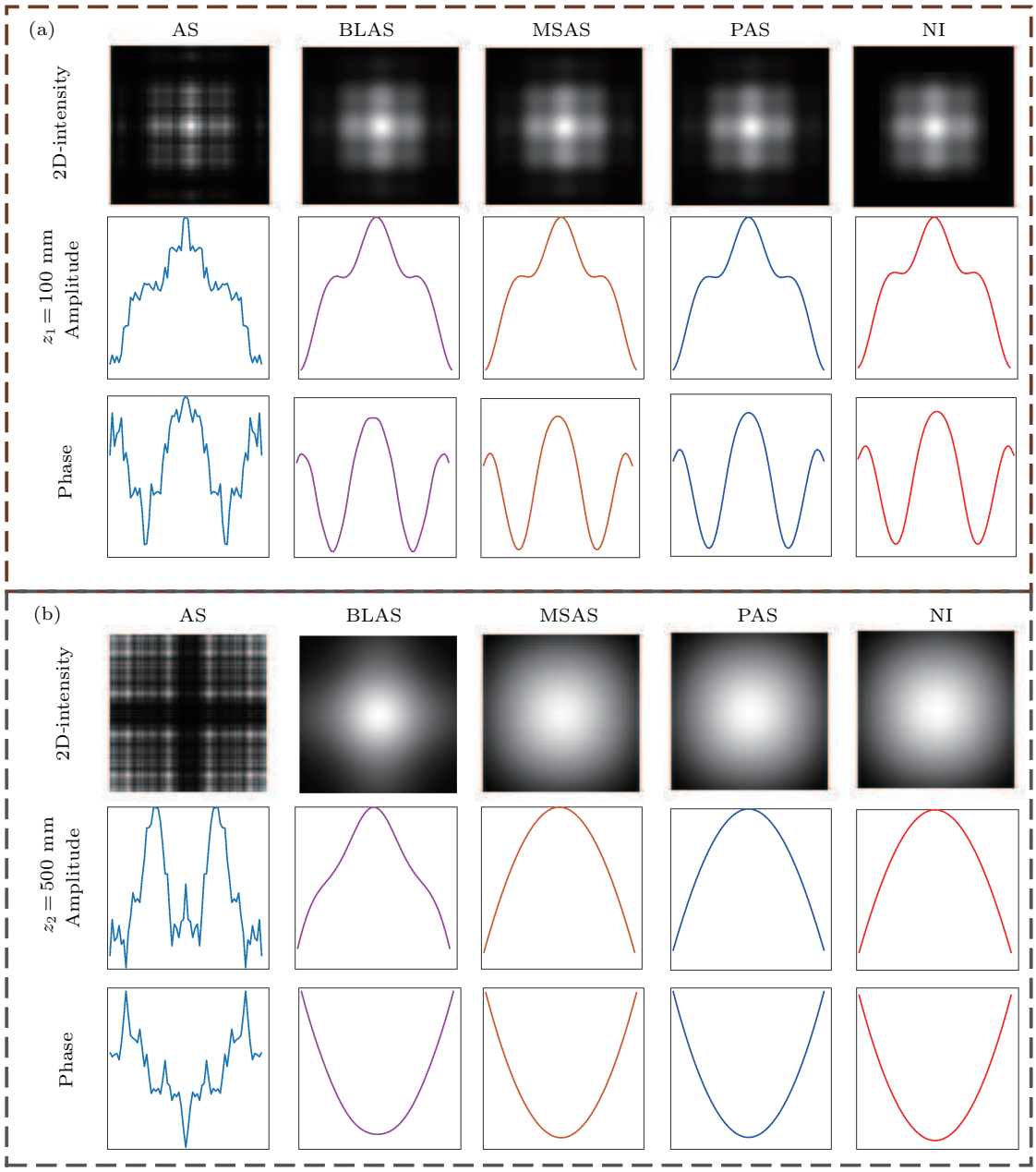


Fig. 7. The 2D-diffraction intensity, 1D-amplitude, and phase using AS, BLAS, MSAS, PAS, and NI in $z_1 = 100$ mm and $z_2 = 500$ mm, respectively. (a) $z_1 = 100$ mm; (b) $z_2 = 500$ mm.

The intensities calculated inversely by MSAS and BLAS under the distances of $z_1 = 100$ mm and $z_2 = 500$ mm are given in Fig. 8. Due to the limitation of the bandwidth in the transfer function, the accuracy of inverse calculation in BLAS decreases with the increase of propagation distance as shown in Figs. 8(a), 8(b), 8(a1), and 8(b1). The application of BLAS in the iterative

phase retrieval technology is limited. But MSAS is not restricted to inverse calculation as shown in Figs. 8(c), 8(d), 8(c1), and 8(d1).

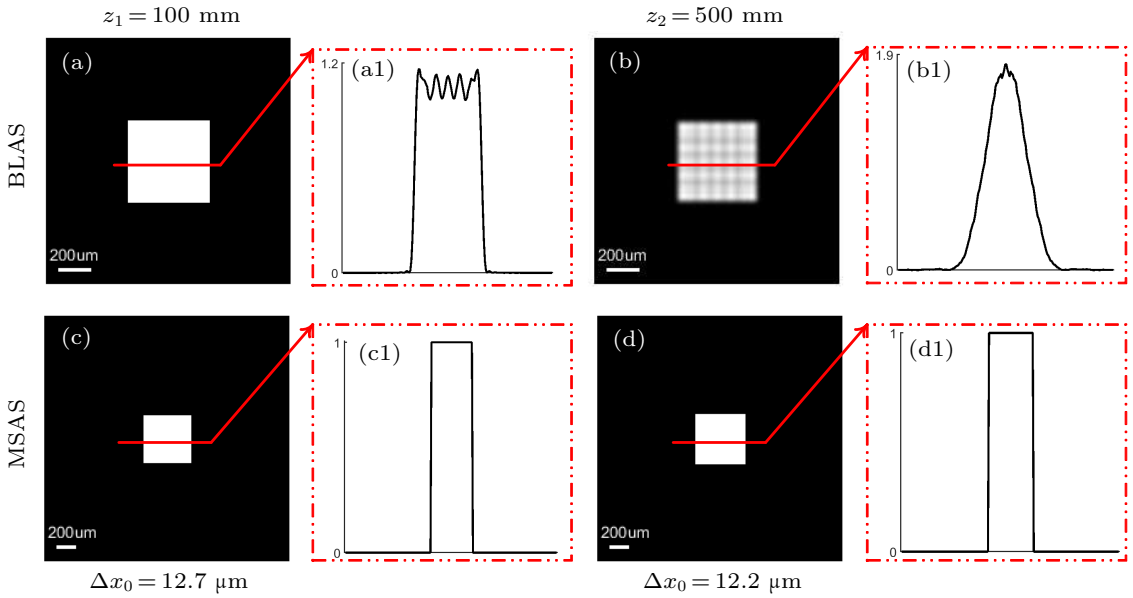


Fig. 8. The 2D-intensity and 1D-intensity using the inverse calculation of BLAS and MSAS under $z_1 = 100$ mm and $z_2 = 500$ mm. BLAS: (a) the inverse result in $z_1 = 100$ mm, (a1) center section view of panel (a); (b) the inverse result in $z_2 = 500$ mm, (b1) center section view of panel (b); MSAS: (c) the inverse result in $z_1 = 100$ mm, (c1) center section view of panel (c); (d) the inverse result in $z_2 = 500$ mm, (d1) center section view of panel (d).

5. Experiment

The experimental setup is shown in Fig. 9. The laser with a wavelength $\lambda = 635$ nm goes through the collimating lens and the pinhole, getting to the CCD. The diameter of the pinhole is 0.5 mm, the pixel size of CCD is $\Delta x = \Delta y = 7.4$ μm with a total number of pixels is 1600×1200. The PV of wavefront error is 0.13λ (the caliber is $\phi = 6$ mm) so that the wavefront in the pinhole can be approximated as a plane wave. The distances between the pinhole and CCD are $z_1 = 113$ mm and $z_2 = 520$ mm, respectively.

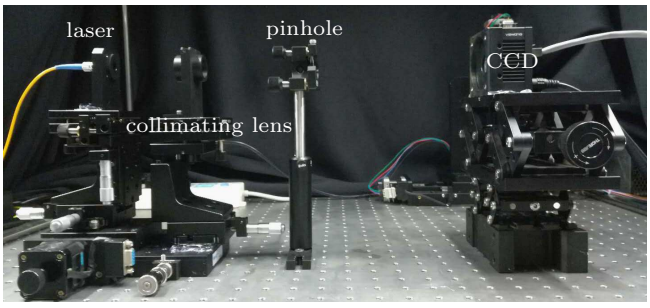


Fig. 9. Experimental setup.

When the distance is $z_1 = 113$ mm, the sampling number in the pinhole plane is $M_{\mathrm{PAS}} \times N_{\mathrm{PAS}} = 1310 \times 1310$ by using PAS. Using MSAS, the sampling interval of pinhole plane is $\Delta x_0 = \Delta y_0 = 16.7$ μm and the sampling number of calculation window is $P \times Q = 512 \times 512$. Similarly, when the distance is $z_2 = 520$ mm, the sampling number using PAS in the pinhole plane is $M_{\mathrm{PAS}} \times N_{\mathrm{PAS}} = 6030 \times 6030$. Using MSAS, the sampling interval of pinhole plane is $\Delta x_0 = \Delta y_0 = 18.1$ μm and the sampling number of calculation window is $P \times Q = 2016 \times 2016$.

Figure 10 shows the diffractive spots of PAS, MSAS, and experiment. The one-dimensional cross-sectional views of MSAS and experiment along the center are shown in Fig. 11. In order to further prove the agreements between simulation by MSAS and experiment, the correlation coefficient c is defined

$$c = \frac{\sum[(I_1 - \bar{I}_1) \cdot (I - \bar{I})]}{\sqrt{\sum (I_1 - \bar{I}_1)^2 \cdot \sum (I - \bar{I})^2}}, \tag{26}$$

where I and $\bar{I}$ represent the experimental intensity and the average experimental intensity of diffraction spot, respectively; I_1 and $\bar{I}_1$ represent the diffraction intensity and the average diffractive intensity calculated by MSAS, respectively.

From Figs. 10(b) and 10(e), there is no periodic artifacts appear in the diffraction spots calculated by MSAS under two distances. Either in Fig. 10 or Fig. 11, MSAS is also highly consistent with the experimental results. And the correlation coefficients of the two in $z_1 = 113$ mm and $z_2 = 520$ mm are $c_1 = 0.9502$ and $c_2 = 0.9992$, respectively. As the propagation distance increases, the correlation coefficients increase because the influence of wavefront aberration is getting smaller. And the calculation time of PAS is about $3.93\times$ and $5.77\times$ of MSAS in $z_1 = 113$ mm and $z_2 = 520$ mm, respectively. Therefore, for long-distance propagation, the calculation of MSAS is accurate and fast.

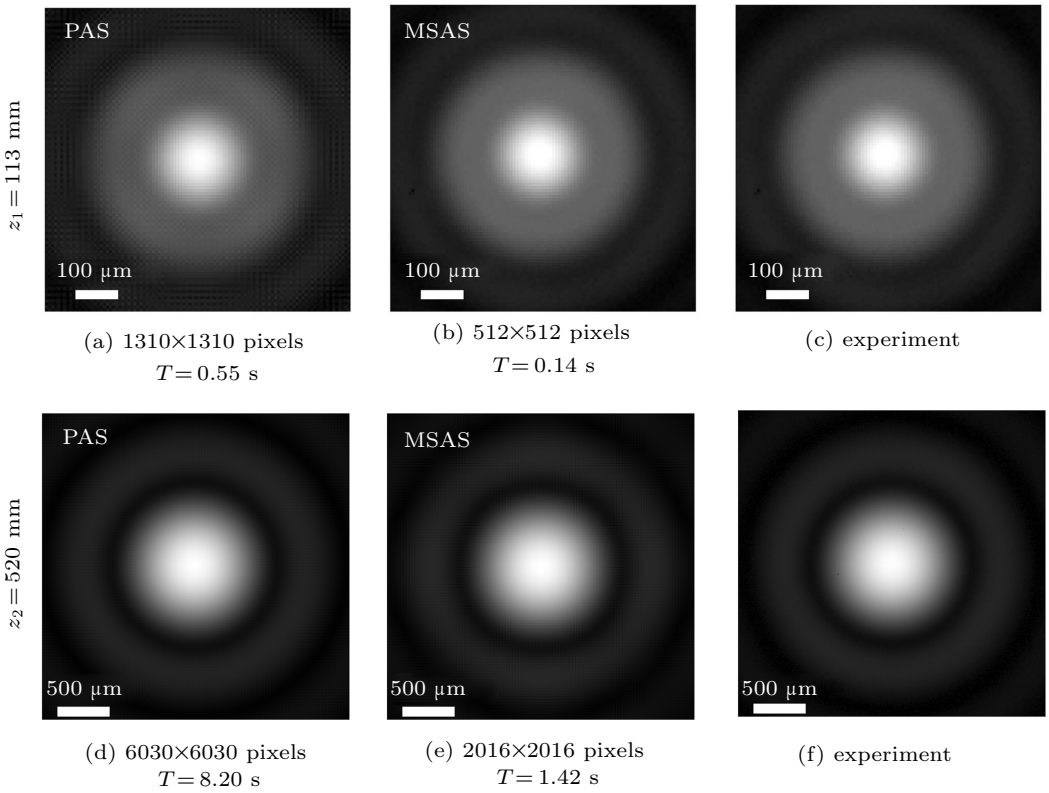


Fig. 10. The diffractive spots of PAS, MSAS, and experiment. Top row: $z_1 = 113$ mm, (a) calculated by PAS, (b) calculated by MSAS, (c) experiment; bottom row: $z_2 = 520$ mm, (d) calculated by PAS, (e) calculated by MSAS, (f) experiment.

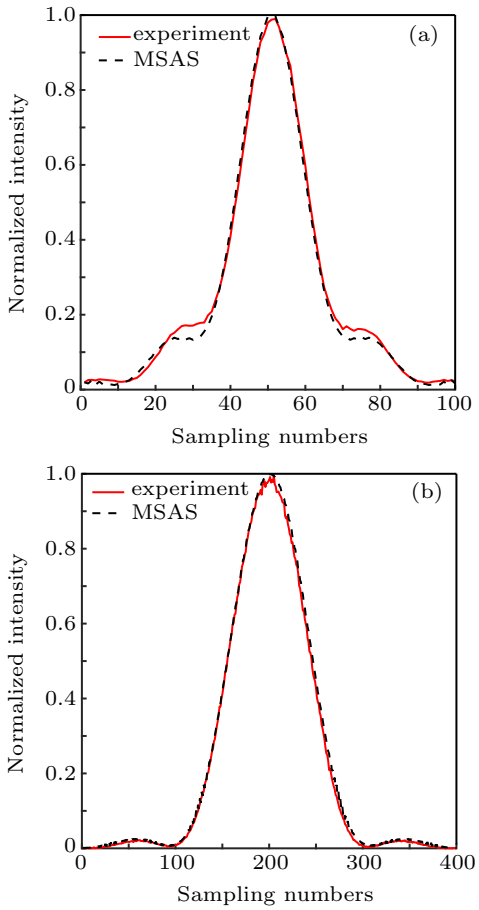


Fig. 11. One-dimensional cross-sectional views of MSAS and experiment along the center: (a) $z_1 = 113$ mm, (b) $z_2 = 520$ mm.

6. Conclusion

In conclusion, a modified scaling angular spectrum (MSAS) method to solve the problem in AS for long-distance propagation is proposed. The method consists of two parts, the scaling calculation and the selection of calculation window. The former is used to freely define the sampling intervals of the input and output planes. The latter is to ensure that MSAS is calculated accurately for the long-distance propagation. It is indicated from the simulation and experiment that MSAS is highly consistent with NI and experimental results, and the calculation speed is faster than PAS. Meanwhile, MSAS does not limit bandwidth in the frequency domain like BLAS, so its accuracy in inverse calculation is much higher than BLAS. Both simulation and experiment prove the correctness of MSAS and it has a great prospect for application in iterative phase retrieval.

References

[1] Maiden A M and Rodenburg J M 2009 *Ultramicroscopy* **109** 1256
[2] Pedrini G, Osten W and Zhang Y 2005 *Opt. Lett.* **30** 833
[3] Pan A and Yao B 2019 *Opt. Express* **27** 5433
[4] Shi Y, Wang Y and Zhang S 2013 *Chin. Phys. Lett.* **30** 054203
[5] Li Z, Zhang J, Liu D and Wang X 2016 *Chin. Phys. Lett.* **33** 024204
[6] Xie Z, Ma H, Qi B, Ren G, Tan Y, He B, Zeng H and Jiang C 2015 *Chin. Phys. Lett.* **32** 124203
[7] Zhou P, Li Y, Liu S and Su Y 2019 *Opt. Express* **27** 8958
[8] Stockmar M, Cloetens P, Zanette I, Enders B, Dierolf M, Pfeiffer F and Thibault P 2013 *Sci. Rep.* **3** 1927

[9] Wang S, Meng X, Wang Y, Yin Y and Yang X 2019 *Chin. Phys. B* **28** 084203
[10] Ou X, Horstmeyer R, Yang C and Zheng G 2013 *Opt. Lett.* **38** 4845
[11] Samuel M and Andrew M 2018 *Opt. Express* **26** 25471
[12] Kreis T M, Adams M and Jueptner W P O 1997 *SPIE Proc.* **3098** 224
[13] Zhang F, Yamaguchi I and Yaroslavsky L P 2004 *Opt. Lett.* **29** 1668
[14] Yu L and Kim M K 2006 *Opt. Lett.* **31** 897
[15] Wang D, Zhao J, Zhang F, Pedrini G and Osten W 2008 *Appl. Opt.* **47** D12
[16] Muffoletto R P, Tyler J M and Tohline J E 2007 *Opt. Express* **15** 5631
[17] Goodman J W 2005 *Introduction to Fourier Optics*, 3nd edn. (Greenwood Village (Colorado): Roberts and Company Publishers) pp. 42–50
[18] Shen F and Wang A 2006 *Appl. Opt.* **45** 1102
[19] Matsushima K and Shimobaba T 2009 *Opt. Express* **17** 19662
[20] Zhang W, Zhang H and Jin G 2020 *Opt. Lett.* **45** 1543
[21] Bluestein L 1970 *IEEE Trans. Audio Electroacoust.* **18** 451
[22] Restrepo J F and Garcia-Sucerquia J 2010 *Appl. Opt.* **49** 6430
[23] Hincapie D, Velasquez D and Garcia-Sucerquia J 2017 *Opt. Lett.* **42** 5294
[24] Shin S and Yu Y 2019 *J. Korean Phys. Soc.* **74** 98
[25] Li J, Peng Z and Fu Y 2007 *Opt. Commun.* **280** 243
[26] Xiao Y, Tang X, Qin Y, Peng H and Wang W 2012 *J. Opt. Soc. Am. A* **29** 2415
[27] Voelz D G and Roggemann M C 2009 *Appl. Opt.* **48** 6132
[28] Xiao Y, Tang X, Qin Y, Peng H and Wang W 2012 *Opt. Lett.* **37** 4943
[29] Veerman J A C, Rusch J J and Urbach H P 2005 *J. Opt. Soc. Am. A* **22** 636
[30] Stamnes J J 1989 *J. Opt. Soc. Am. A* **6** 1330